Key Points:
- Interannual variability in the mesoscale eddy field in the Canada Basin is examined between 2005 and 2015
- The highest numbers of eddies are in the western and southern portions of the basin
- The number of lower halocline eddies increased from the period 2005-2012 to 2013-2014

Correspondence to:
M. Zhao,
mengnan.zhao@yale.edu

Evolution of the eddy field in the Arctic Ocean's Canada Basin, 2005–2015

Mengnan Zhao[1], Mary-Louise Timmermans[1], Sylvia Cole[2], Richard Krishfield[2], and John Toole[2]

[1]Department of Geology and Geophysics, Yale University, New Haven, Connecticut, USA, [2]Department of Physical Oceanography, Woods Hole Oceanographic Institution, Woods Hole, Massachusetts, USA

Abstract The eddy field across the Arctic Ocean's Canada Basin is analyzed using Ice-Tethered Profiler (ITP) and moored measurements of temperature, salinity, and velocity spanning 2005 to 2015. ITPs encountered 243 eddies, 98% of which were anticyclones, with approximately 70% of these having anomalously cold cores. The spatially and temporally varying eddy field is analyzed accounting for sampling biases in the unevenly distributed ITP data and caveats in detection methods. The highest concentration of eddies was found in the western and southern portions of the basin, close to topographic margins and boundaries of the Beaufort Gyre. The number of lower halocline eddies approximately doubled from 2005–2012 to 2013–2014. The increased eddy density suggests more active baroclinic instability of the Beaufort Gyre that releases available potential energy to balance the wind energy input; this may stabilize the Gyre spin-up and associated freshwater increase.

1. Introduction

Mesoscale eddies with horizontal length scales around 10 km are prevalent features across the Arctic Ocean, and their characteristics and dynamics have been well studied since Arctic eddy features were first described by *Hunkins* [1974] and later summarized by *Manley and Hunkins* [1985]. Recent high-resolution temperature and salinity measurements from drifting Ice-Tethered Profilers (ITPs) have enabled an Arctic-wide study of the eddy field over the past decade [*Zhao et al.*, 2014]. Over the entire Arctic basin, anticyclonic eddies were shown to dominate over cyclones (by a ratio of 25 to 1), and most eddies had anomalously cold cores and were confined to the halocline; lifetimes were estimated to be weeks to years [*Zhao et al.*, 2014]. Eddies are generally thought to be translated by background mean flows, after having been formed by baroclinic instability of boundary currents or fronts [e.g., *Spall et al.*, 2008; *Timmermans et al.*, 2008]. Eddy horizontal scales are of the same order as the first baroclinic Rossby deformation radius, and their vertical scales are inversely related to the ambient stratification [*Carpenter and Timmermans*, 2012; *Zhao and Timmermans*, 2015].

Eddies have relevance to ocean stirring and mixing [e.g., *McWilliams*, 2008], halocline ventilation and maintenance [e.g., *Spall et al.*, 2008], transport of nutrients and chemical tracers in the Arctic Ocean [e.g., *Nishino et al.*, 2011], and vertical transfer of ocean heat [e.g., *Bebieva and Timmermans*, 2016]. The role of eddies in the energetics of wind-driven ocean gyres has long been recognized [e.g., *Holland*, 1978]. The large-scale ocean circulation in the Canada Basin (the focus region of our study) is the wind-driven Beaufort Gyre forced by the prevailing anticyclonic atmospheric circulation [*Proshutinsky and Johnson*, 1997; *Proshutinsky et al.*, 2002]. The basic water column structure in the Beaufort Gyre/Canada Basin region consists of a thin fresh mixed layer separated from a relatively warm Atlantic Water layer (centered around 400 m depth) by a halocline (with both warm and cool portions) between ~50 m and ~250 m depths [e.g., *Aagaard et al.*, 1981]. The Beaufort Gyre system, coupling the atmosphere, sea ice, and ocean layers, regulates freshwater content and stratification in this sector of the Arctic Ocean [*Proshutinsky et al.*, 2009a]. A strong anticyclonic wind pattern has dominated from 1997 to 2015 [e.g., *Proshutinsky et al.*, 2015] driving freshwater accumulation via Ekman convergence, with complex influences due to changing river runoff and growth and decay of sea ice [e.g., *Proshutinsky et al.*, 2009b; *Morison et al.*, 2012; *Krishfield et al.*, 2014]. The release of this freshwater would have consequences not only to Arctic Ocean stratification and sea ice cover but also to stratification, air-sea fluxes, and circulation in the subpolar oceans [e.g., *Proshutinsky and Johnson*, 1997; *Dickson et al.*, 1988]. Mesoscale eddies are no doubt an important mechanism for release of available potential energy in the wind-driven Beaufort Gyre and likely offset freshwater accumulation by being shed at the gyre boundaries. *Manucharyan and Spall* [2015],

for example, used an idealized eddy-resolving model and fundamental theory to show how a steady balance (between freshwater content in the Beaufort Gyre and steady wind forcing) may be maintained via the continuous generation of eddies by baroclinic instability at the sloping isopycnal surfaces of the gyre. Employing an idealized eddy-permitting model, *Yang et al.* [2016] further showed that eddies play a role in the Beaufort Gyre vorticity balance; in a steady state, eddy vorticity flux is the main balance of a constant wind stress curl input.

Motivated by the relevance of eddies to Beaufort Gyre energetics and dynamics, in this paper we take advantage of the eddy-resolving, basin-wide distribution of ITP and mooring data taken during 2005–2015 to examine the interannual and spatial variability in the eddy field in this region. A major thrust of our analysis is to examine the change in eddy density with constraints due to the temporal and spatial limitations of the data. Measurements are introduced in section 2. Section 3 describes the detection and characterization of eddies, as well as factors that may influence the resulting statistics. The varying eddy numbers and eddy types over the past decade are presented in section 4, and these are set in context with the uneven temporal and spatial distribution of measurements. In section 5, we summarize and discuss our findings.

2. ITP and Mooring Measurements

ITP data constitute the primary measurements used in this study. An ITP is composed of a surface buoy deployed on an ice floe with a tether extending from the base of the buoy along which a conductivity-temperature-depth (CTD) profiling unit makes repeated measurements of pressure, temperature, and salinity between ~7 m and ~750 m depth. CTD data (sampled at 1 Hz) have a vertical resolution of about 25 cm, and these are returned via satellite along with hourly GPS position information [*Krishfield et al.*, 2008; *Toole et al.*, 2011]. Between two and six profiles are returned each day, yielding a horizontal spacing between profiles of a few kilometers or less; ocean velocity measurements confirm that typical sea ice drift speeds (order 10 cm s^{-1}) are an order of magnitude faster than typical ocean velocities in the halocline [e.g., *Cole et al.*, 2014]. Six ITPs were also equipped with velocity sensors (ITP-V), which sampled in 2009–2010 and 2013–2015 (deployed to study the marginal ice zone: http://www.apl.washington.edu/project/project.php?id=miz), returning horizontal velocity profiles in addition to CTD data [see *Cole et al.*, 2014, 2015]. Here we analyze data (1 m averaged in the vertical) obtained between 17 August 2005 and 31 December 2015 from 39 ITP systems in the Canada Basin (in the sector between 170°W and 120°W, and 70°N and 85°N; Figure 1). Only profiles with a minimum depth less than 15 m and a maximum depth of at least 150 m are used in this study. Most eddy cores are shallower than 150 m, and even eddies at deeper levels still have an isopycnal expression above 150 m.

In addition to ITP data, measurements from four moorings deployed under the Beaufort Gyre Exploration Project (BGEP, http://www.whoi.edu/beaufortgyre/data) between mid-2003 and mid-2014 are also analyzed. Moorings are deployed at four sites across the Beaufort Gyre (Figure 1a). Each mooring system included a McLane Moored Profiler that returned profiles of horizontal velocity, temperature, salinity, and pressure. A pair of upgoing/downgoing profiles (separated by 6 h) was returned every other day; data were processed to a vertical resolution of 2 dbar. The shallowest moored measurement varies from about 50 m to 90 m (depending on the mooring and sampling period), and the deepest measurements were to 2050 m [*Proshutinsky et al.*, 2009b]. For consistency with ITP measurements, we consider only mooring measurements to 750 m and address the shallow upper bound discrepancy between the ITPs and moorings in section 4.1.

3. Eddy Detection and Sampling Biases

Eddy detection methods are as described by *Zhao et al.* [2014] and *Zhao and Timmermans* [2015]: a mesoscale eddy is identified based on isopycnal displacements in addition to the presence of a temperature anomaly (e.g., Figure 1d). At least four profiles along an approximately straight ITP drift track through an eddy feature are required for confirmation of an eddy. An eddy center is estimated to be the location of most extreme isopycnal displacement and core depth to be the level of maximum temperature anomaly. Either side of the center profile, isopycnal displacements decay to near-horizontal values characterizing the ambient water. Eddy diameter is defined to be the distance between the closest profiles that exhibit isopycnal displacements ≲5 m with respect to the ambient water stratification. Eddy center position and diameter will be in error when an ITP skirts the outer edge of an eddy; however, the error in diameter is generally less than around 15% (as discussed in *Timmermans et al.* [2008] and *Zhao et al.* [2014]).
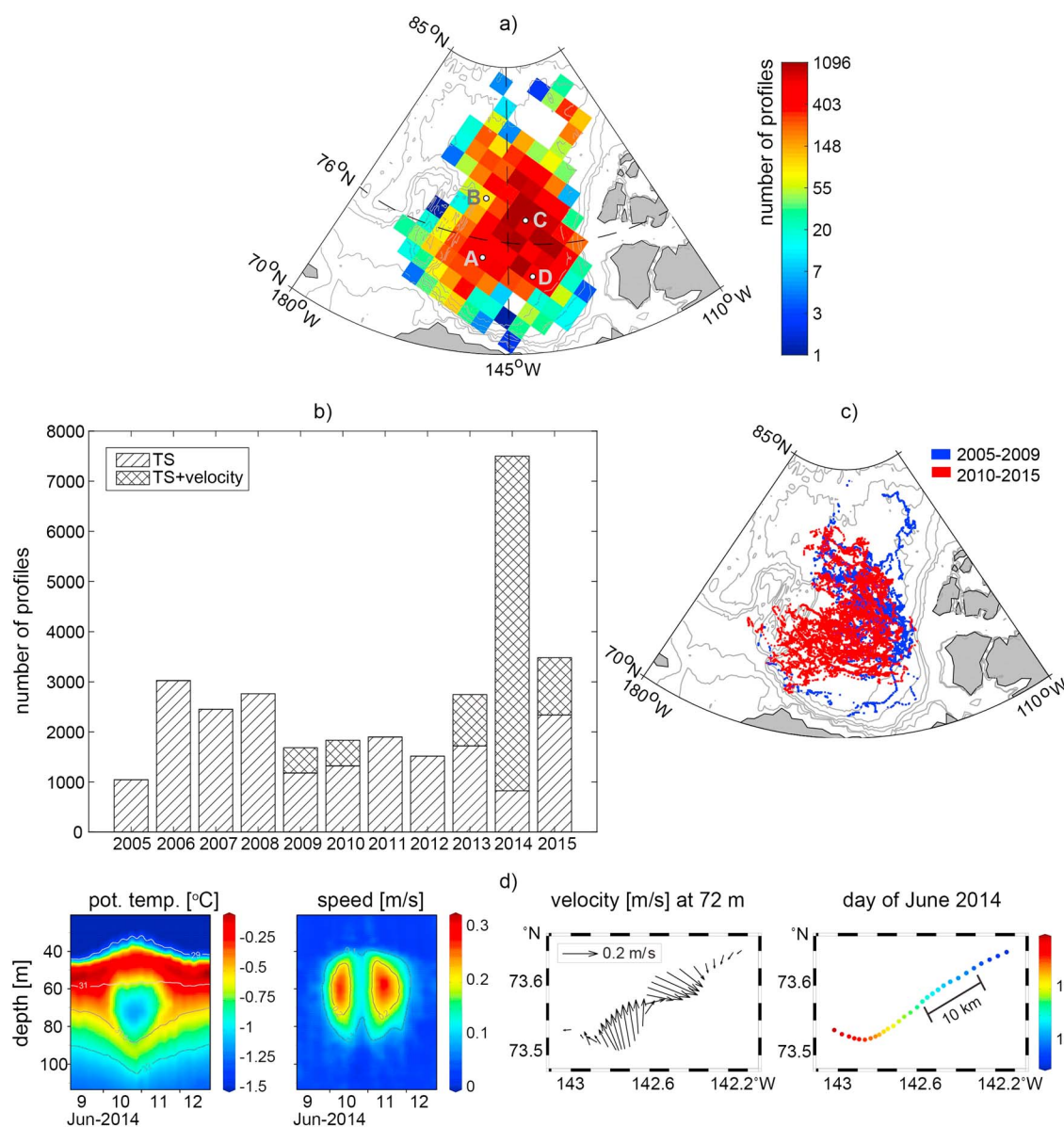
Figure 1. (a) Number of profiles used in this analysis per 100 km × 100 km cell in the Canada Basin between 2005 and 2015 from all ITPs. The locations of the four BGEP moorings (A, B, C, and D) are also indicated. Dashed lines divide the basin into four sectors corresponding to each of the four moorings. (b) Number of profiles with measurements from ITP-Vs (including horizontal velocity in addition to temperature and salinity) and ITPs (only temperature and salinity) in each year. (c) The locations of all ITP measurements from 2005 to 2009 (blue) and 2010 to 2015 (red). (d) A typical upper halocline eddy (core salinity <32, sampled by ITP 77 in 2014 in the southern portion of the basin). First panel: potential temperature (°C)-depth (m) section overlaid with salinity contours; second and third panels: velocity magnitude (m/s)-depth (m) section and the velocity field at the eddy core depth; fourth panel: ITP drift track through the eddy showing dates and horizontal scale.

Velocity data provide an additional way to identify eddies based on the presence of high (azimuthal) speeds. The criterion here is that maximum eddy speeds must be larger than a threshold of 10 cm/s (i.e., much larger than typical background speeds of a few cm/s; see *Zhao and Timmermans* [2015]) and decrease away from the eddy core. When an ITP transects the core of an eddy (or when the inner core of an eddy passes a mooring), two speed maxima are identified, and this structure is always accompanied by characteristic isopycnal displacements and a core temperature anomaly from the ambient water column. When an ITP skirts the outer edge of an eddy (or an eddy edge passes a mooring), it is possible that only one speed maximum is recorded. In this case, the ITP/mooring may not record pronounced isopycnal displacements nor a core temperature anomaly. Velocity measurements also aid in confirming eddies when the ITP drift tracks are

circuitous. A small fraction of eddies (several percent) appear in the data record that cannot be detected without velocity data. In section 4 we take this into consideration in our interpretation of interannual variability of the eddy field given the uneven distribution of velocity measurements.

The possibility of repeat eddy encounters, which can arise when an ITP drifts circuitously around a localized region and samples the same eddy more than once, is another factor that may influence the statistics. For example, ITP 77 appears to have sampled the same eddy twice on 11 July and again on 17 July 2014. Both eddy encounters showed similar core depths (≈245 m), core potential temperature around −1.55°C, and salinity around 33.95. Maximum measured velocities were about 40 cm/s at both encounters. We estimate radii (following *Zhao and Timmermans* [2015]) to be 6.7 km and 7.1 km, respectively. The similar eddy properties sampled less than 1 week apart in the same general vicinity may indicate that these two encounters are of the same eddy. This would imply an eddy advection speed of about 0.7 cm/s in a northeast direction consistent with the eddy being transported by the general Beaufort Gyre circulation [see *Proshutinsky et al.*, 2009b]. A total of 19 eddies (7% of the total) were considered to have been sampled twice between 2005 and 2015. In these cases, one of the encounters was not included in the population statistics.

Varying horizontal ITP profile spacing may also contribute to sampling biases; yearly mean profile spacing varies between 1.8 km and 3.6 km over the decade. Since a minimum of four profiles is required for the identification of an eddy, the cumulative distance between the first and last of these four profiles dictates the minimum eddy diameter that can be identified, i.e., smaller profile spacing can capture smaller eddies or be more likely to identify an eddy encounter when the ITP transits its outer core, and this will be considered in our interpretation.

4. Interannual and Spatial Variability in the Eddy Field

Between 2005 and 2015, three cyclones and 240 anticyclones are identified in ITP measurements, including five anticyclones with core depths deeper than 300 m—Atlantic Water eddies (Figure 2). The remainder of the anticyclones was located in the halocline (235 in total). Of these, 170 had a single, anomalous cold core; 23 had a single, anomalous warm core; 30 had stacked double cores (both anomalously cold and warm) [see *Zhao et al.*, 2014]; and 12 anticyclones showed no temperature anomaly (these were detected from the velocity fields). The spatial distribution of eddies (Figure 2a) may be biased due to the uneven distribution of ITP profiles from year to year (Figure 1a). Nevertheless, it appears that the southern and western portions of the basin exhibit greater eddy density (Figure 2b). Indeed, our analysis of BGEP mooring data supports this as will be shown below.

The total number of eddies observed each year (normalized by the cumulative distance sampled by ITPs over the course of that year) shows interannual variability with eddy encounters (per 1000 km sampled) increasing in the period from 2012 to 2014, although this is also observed with a concurrent increase in total distance sampled in those years (Figure 2c).

The interannual variability in eddy numbers may be influenced by the spatial coverage of ITP measurements (Figure 1a), the number of measurements in each year, the additional velocity measurements (Figure 1b), the cumulative distance sampled in each year (Figure 2c, red line), and the horizontal profile spacing (Figure 2c, green numbers). Intensive ITP measurements in 2014 were concentrated in the western basin, and the average profile spacing was a minimum at this time owing in part to frequent profiling. In addition, five ITPs were equipped with velocity sensors in 2014, resulting in 11 more eddies being identified (some 11% of all eddies in 2014) than if velocity measurements were not available. All these factors contribute to higher eddy numbers in 2014.

Given the above potential biasing factors, we exclude those halocline eddies that were only identified with velocity measurements (Figure 2c, grey bars). Years with larger mean profile spacing may return fewer small eddies or miss eddies whose outer cores are transected by ITPs. In light of the mean profile spacing in each year (Figure 2c, green numbers) and our requirement that a minimum of four profiles are needed for eddy detection, nearly all ITP data sets in the archive are capable of detecting eddies larger than about 10 km. The present analysis therefore restricts attention to eddies larger than 10 km to minimize sampling bias related to different ITP profiling frequency and drift rates (*Zhao et al.* [2014] show that halocline eddies have diameters consistent with the first baroclinic deformation radius, ~12 km in this region). This yields a conservative
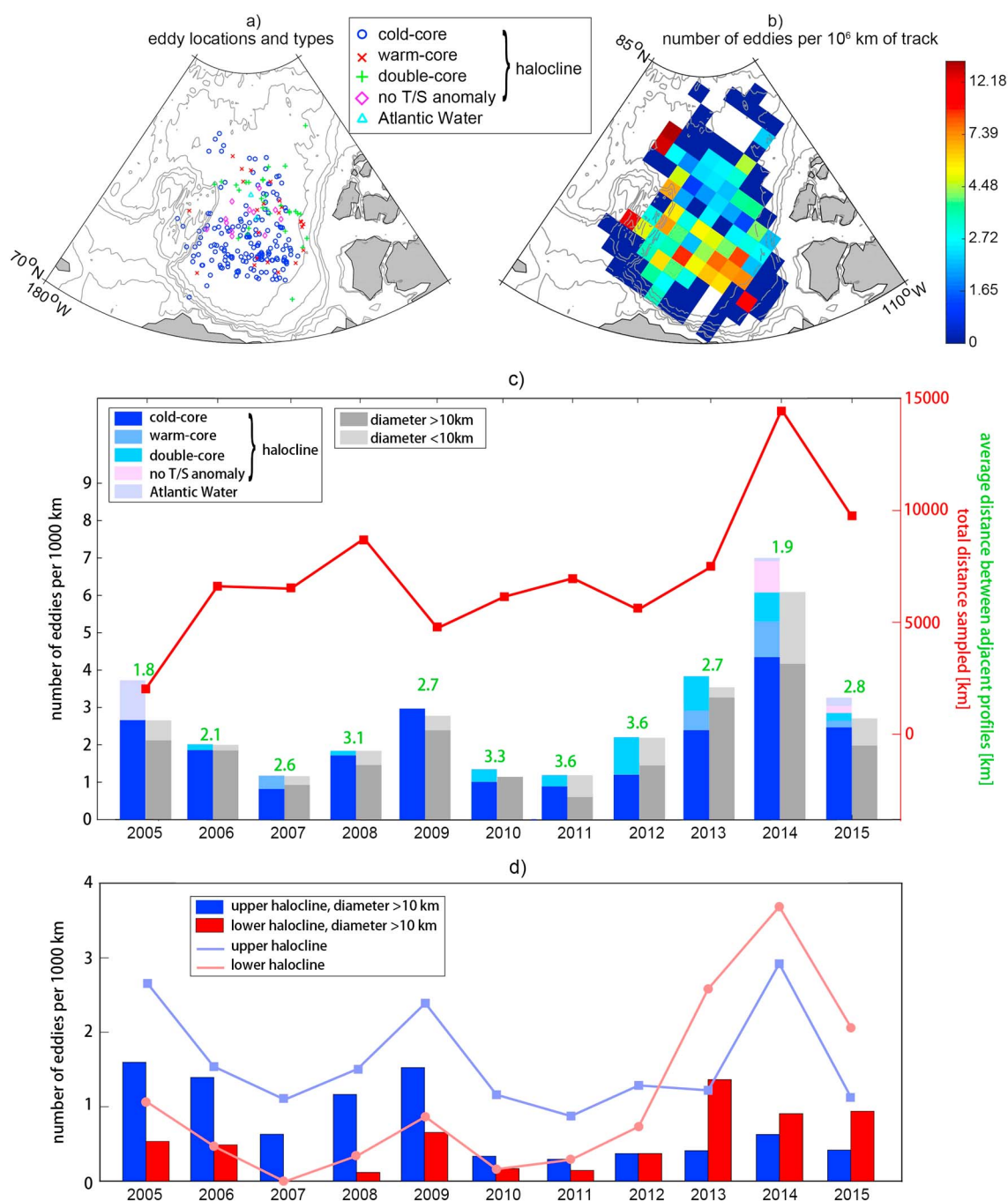
Figure 2. (a) Eddy locations and types sampled between 2005 and 2015 from all ITPs. (b) Number of eddies per 10^6 km of ITP drift track in each 100 km×100 km cell. (c) Time series of the number of anticyclonic eddies per 1000 km (bars) and total cumulative (along track) distance (red line) sampled from 2005 to 2015. Green numbers indicate the average distance (km) between adjacent ITP profiles (i.e., average horizontal resolution). Colored bars include all types of anticyclonic eddies. Grey bars include only halocline anticyclonic eddies detected based on temperature and salinity fields and not velocity. (d) Time series of the number of upper halocline eddies (blue, core salinity <32) and the number of lower halocline eddies (red, core salinity >32) per 1000 km. The lines include all halocline anticyclonic eddies identified only from temperature and salinity measurements, and the bars include only eddies larger than 10 km in diameter.

estimate for eddy numbers (Figure 2c, dark grey bars), which shows the same general variability as before accounting for biases, including 5.2 times as many eddies in 2014 than in 2011.

Considering only eddies larger than 10 km over the period, more upper halocline eddies (having core salinities ≲32 and core depths ≲80 m) are sampled in 2005–2009 (Figure 2d, blue bars), while significantly more lower halocline eddies (having core salinities ≳32 and core depths ≳80 m) are observed in 2013–2015 (Figure 2d, red bars). This trend may be biased by spatial sampling distributions since ITP measurements in the earlier group of years are generally concentrated more in the northern and eastern portions of the basin (Figure 1c) close to a surface front separating Eurasian and Canadian basin waters—believed to generate the upper halocline eddies studied by *Timmermans et al.* [2008] and where the majority of this type of eddy are found [*Zhao et al.*, 2014]. These upper halocline eddies are closer to the surface ocean and sea ice and may have shorter lifetimes than lower halocline eddies due, for example, to spin-down mechanisms associated with ice-ocean stresses [*Ou and Gordon*, 1986], further decreasing the possibility of being found in the western basin further from their origins. On the other hand, ITP drift tracks in later years concentrate in the western part of the basin (Figure 1c) where most of the lower halocline eddies, believed to originate predominantly from boundary currents in the southern basin, were identified [*Zhao et al.*, 2014]. Therefore, we cannot draw reliable conclusions without taking into account the spatial biases in sampling, which will be further discussed with the aid of mooring data in the next section.

4.1. Using Moored Measurements to Further Constrain the Eddy Field

The fixed mooring measurements in four quadrants of the Beaufort Gyre region provide an essential measure of the spatial variability of the eddy field, which may be examined in context with the spatial distribution of ITP measurements to quantify spatial sampling biases. Given that the moorings sample no shallower than approximately 50 m, this analysis can be done only for the lower halocline eddy field (i.e., eddies with core salinity >32).

The western moorings (moorings A and B) exhibit higher depth-integrated kinetic energy (KE) than the eastern moorings C and D (Figures 3a and 3b); depth-integrated KE is computed by $\int \frac{1}{2} \rho \left(u^2 + v^2 \right) dz$ (J/m^2), where the integration is between 90 m and 750 m depths and u and v are the instantaneous horizontal velocity components (mesoscale eddies dominate KE in the mooring records) [*Zhao and Timmermans*, 2015]. There is clearly a more active eddy field near the western basin bathymetric and Beaufort Gyre boundary [see *Zhao et al.*, 2014; *Zhao and Timmermans*, 2015]. This spatial distribution is generally consistent with ITP data (Figure 2b). We conclude that the southern and western portions of the basin contain more lower halocline eddies than the northern and eastern portions of the basin.

With respect to temporal variability, the mooring data indicate no apparent seasonal signal in the eddy field (neither in eddy numbers nor in the depth-integrated KE). Given the eddy census of *Zhao et al.* [2014], it is likely that most of the observed eddies are far from their origins (i.e., they propagate long distances before being sampled by ITPs or moorings). This masks any temporal eddy signals that are shorter than interannual. An assessment of interannual variability of the eddy field measured by ITPs can be improved by taking into account the spatial distribution of the eddy field that is evident in the moored measurements. To do this, we make the assumption that the eddies recorded at each mooring are regionally representative and divide the basin into four sectors with boundaries of 145°W and 76°N (Figure 1a). Considering only lower halocline eddies, we find that on average, for every 12 eddies at Mooring A, there were 11 eddies at Mooring B, 1 eddy at Mooring C, and 4 eddies at Mooring D; this is equivalent to a ratio that considers elevated levels of depth-integrated KE. We use this ratio to estimate the number of eddies in each sector based on ITP observations in one sector (For example, in 2006, 3.2 eddies per 1000 km are identified in ITP measurements from sector B. Using this number, we estimate the number of eddies per 1000 km in sectors A, C, and D to be 3.5, 0.3, and 1.2, respectively.) Thus, there are multiple estimates of the number of eddies in each sector during years in which ITPs detected eddies in more than one sector. We average these estimates with vertical bars denoting maximum and minimum values (Figure 3c). In the calculation, we consider only lower halocline eddies with diameters larger than 10 km and those which can be identified in the absence of velocity data.

It must be emphasized that this method assumes that the relative spatial distribution of eddies remains the same over time. Ideally, we would have some reasonable representation of how the ratio of eddy numbers in each of the four sectors changes from year to year, but this is not possible with the limited measurements. In the few years that the data allow for the estimation of ratios in a single year, we find that these ratios do
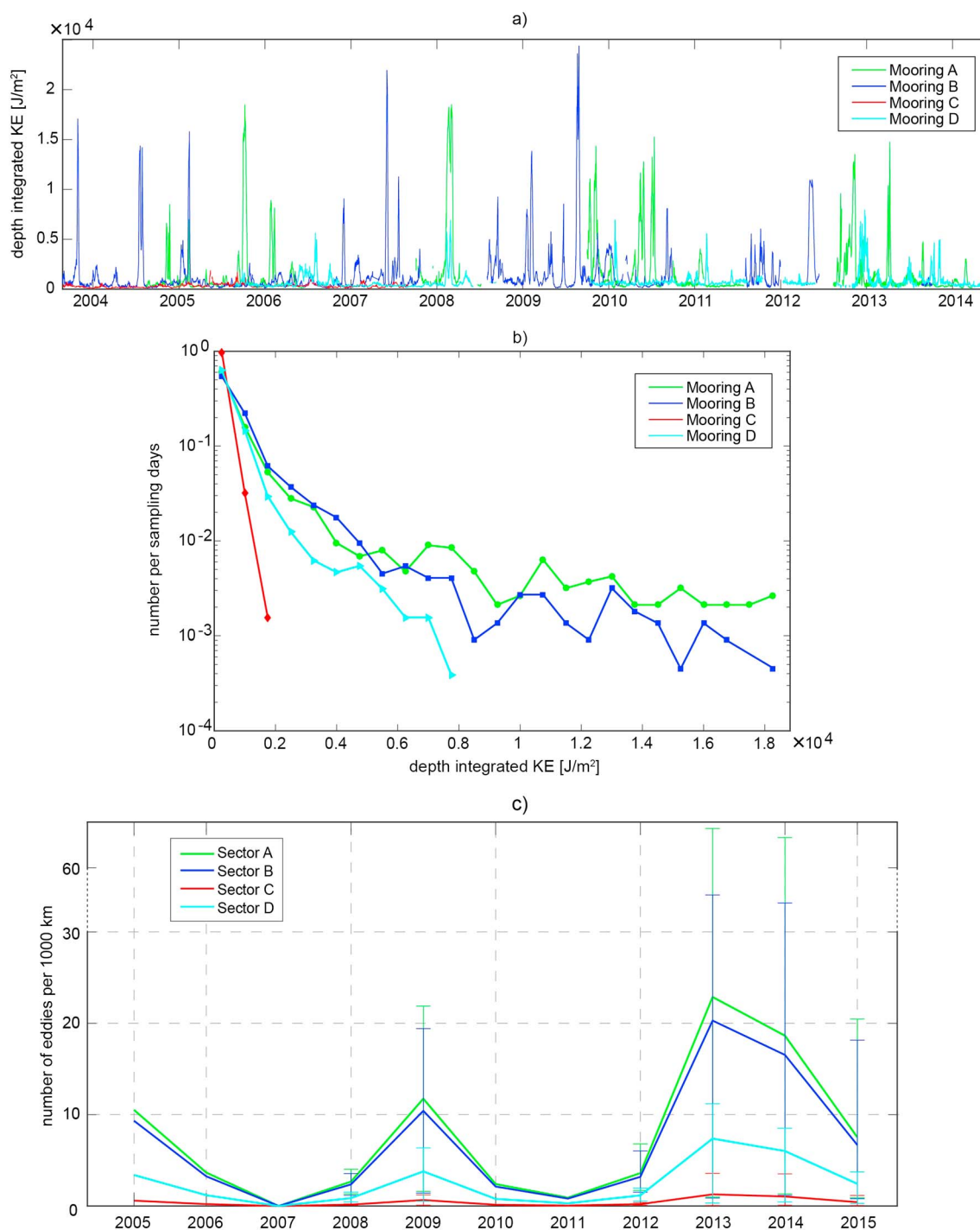
Figure 3. (a) Depth-integrated kinetic energy (KE) from 90 m to 750 m (see text) from all mooring measurements between 2003 and 2013. The absence of measurements indicates gaps in the mooring records. (b) A histogram of depth-integrated KE (J/m²) between 90 m and 750 m for a bin size of 750 J/m² normalized by the total number of sampling days. (c) The number of lower halocline eddies per 1000 km estimated from ITP data in each of the four sectors accounting for the spatial variability indicated by the moorings (see text). Vertical bars indicate the minimum and maximum estimates when ITP measurements in 1 year cover more than one of the four sectors.

not differ appreciably from the mean values over the record. Over the course of the record, the time series of depth-integrated KE (Figure 3a) shows consistently higher KE at the two western moorings and comparatively low eddy activity at the eastern moorings. This is consistent with the general basin bathymetry (and geometry) and circulation patterns in the Beaufort Gyre and boundary current system, where the majority of eddies are believed to originate. Although it has some shortcomings, the method above allows for some account of the spatial biases introduced by interannual variability in ITP drift locations. The result is a significantly greater lower halocline eddy density in the 2013–2014 periods compared to previous years (Figure 3c). This is consistent with the more active eddy field (at least with respect to lower halocline eddies) found in only the ITP data (Figure 2d, red bars).

5. Summary and Discussion

Analysis of ITP and moored measurements over the decade 2005–2015 reveals highly timely information about the mesoscale eddy field in the Beaufort Gyre region during a time of significant change in wind-forcing and freshwater storage. The eddy field is predominantly anticyclonic with eddies concentrated in the southwestern part of the basin. Approximately 60% more eddies were found there than in the northern and eastern portions of the basin. The period 2013–2014 shows a marked increase in eddy activity compared to the preceding 8 years, with twice as many eddies in the latter period. We have reasonable confidence in the statistics having taken into account the following factors: Eddies that are identified from velocity measurements alone have been excluded because the additional velocity measurements are only available in some years; only eddies with diameter larger than 10 km are included to account for interannual variations in ITP profile spacing; fixed mooring measurements are used to account for spatial sampling biases of the eddy field by drifting ITPs.

The relationship between the recent intensification of the Beaufort Gyre and freshwater storage variability in the region [*Krishfield et al.*, 2014] may be consistent with the enhanced eddy activity in recent years, particularly in the western sector of the basin where the Northwind Ridge topography and Beaufort Gyre boundary coincide. It may be that under strengthening wind stress curl, isopycnal slopes at the gyre boundaries steepen, giving rise to an increase in available potential energy. Baroclinic instability ensues, and eddies are shed in a regulating mechanism that releases available potential energy. *Holland* [1978] assesses this in an idealized wind-driven gyre model and shows that up to 86% of the wind energy input is transferred to the mesoscale eddy field through this process. One possible scenario for the Beaufort Gyre may be a steady balance between its freshwater content and wind forcing [*Manucharyan and Spall*, 2015]. Additional observations are needed to quantify these relationships in the Beaufort Gyre and to understand, for example, the role that eddies play in the stabilization of Beaufort Gyre freshwater content after 2008 [*Krishfield et al.*, 2014]. Besides its relevance to the energetics of the Beaufort Gyre, the more active eddy field in recent years additionally suggests increased shelf-basin exchange, especially of winter-transformed Pacific-origin water which gives rise to the lower halocline eddies [*Pickart et al.*, 2005], and an increased role of eddies in ventilating the halocline. The role of these halocline eddies (having origins in basin boundary currents) on the large-scale energetics of the gyre requires investigation.

Very shallow eddies and smaller eddies (less than 10 km in diameter) that could not be examined here are no doubt another key element of Beaufort Gyre energetics. Indeed, it may be that eddy fluxes from the Beaufort Gyre are dominated by surface-intensified eddies. We can only speculate that the eddy field analyzed here is representative of all eddy types, while the details should be an important focus of future observational and numerical studies.

Eddies observed here are generally thought to have long lifetimes (up to several years) [see, e.g., *Zhao et al.*, 2014]. Our conclusions regarding eddy interannual variability only account for the change in the eddy field present in the basin from year to year. The measurements cannot be used to infer the numbers of eddies generated in each year, which of course more directly reflects the gyre instability. Additional observations (analyzed jointly with high-resolution numerical simulations), particularly in the basin boundary regions, are needed to examine the role of seasonal variability and improve estimates of interannual variability. One of the next challenges in Arctic Ocean simulations is to correctly model interannual variability of the highly spatially and temporally varying eddy field. Sustained observations of eddies and eddy kinetic energy are necessary for comparison to models.

References

Aagaard, K., L. K. Coachman, and E. Carmack (1981), On the halocline of the Artic Ocean, *Deep Sea. Res.*, *28*, 529–545, doi:10.1016/0198-0149(81)90115-1.

Bebieva, Y., and M.-L. Timmermans (2016), An examination of double-diffusive processes in a mesoscale eddy in the Arctic Ocean, *J. Geophys. Res. Oceans*, *121*, 457–475, doi:10.1002/2015JC011105.

Carpenter, J., and M.-L. Timmermans (2012), Deep mesoscale eddies in the Canada Basin, Arctic Ocean, *J. Geophys. Res.*, *39*, L20602, doi:10.1029/2012GL053025.

Cole, S. T., M.-L. Timmermans, J. M. Toole, R. A. Krishfield, and F. T. Thwaites (2014), Ekman veering, internal waves, and turbulence observed under Arctic sea ice, *J. Phys. Oceanogr.*, *44*(5), 1306–1328, doi:10.1175/JPO-D-12-0191.1.

Cole, S. T., F. T. Thwaites, R. A. Krishfield, and J. M. Toole (2015), Processing of velocity observations from ice-tethered profilers, paper presented at OCEANS'15 MTS/IEEE, pp. 1–10, IEEE, Washington, 19–22 Oct.

Dickson, R. R., J. Meincke, S. A. Malmberg, and A. J. Lee (1988), The great salinity anomaly in the northern North Atlantic 1968–1982, *Prog. Oceanogr.*, *20*, 103–151, doi:10.1016/0079-6611(88)90049-3.

Holland, W. R. (1978), The role of mesoscale eddies in the general circulation of the ocean-numerical experiments using a wind-driven quasi-geostrophic model, *J. Phys. Oceanogr.*, *3*, 363–392.

Hunkins, K. L. (1974), Subsurface eddies in the Arctic Ocean, *Deep Sea Res.*, *21*, 1017–1033, doi:10.1016/0011-7471(74)90064-3.

Krishfield, R., J. Toole, A. Proshutinsky, and M.-L. Timmermans (2008), Automated ice-tethered profilers for seawater observations under pack ice in all seasons, *J. Atmos. Oceanic Technol.*, *25*(11), 1092–2105, doi:10.1175/2008JTECHO587.1.

Krishfield, R., A. Proshutinsky, K. Tateyama, W. Williams, E. Carmack, F. McLaughlin, and M.-L. Timmermans (2014), Deterioration of perennial sea ice in the Beaufort Gyre from 2003 to 2012 and its impact on the oceanic freshwater cycle, *J. Geophys. Res. Oceans*, *119*, 1271–1305, doi:10.1002/2013JC008999.

Manley, T. O., and K. L. Hunkins (1985), Mesoscale eddies in the Arctic Ocean, *J. Geophys. Res.*, *90*, 4911–4930.

Manucharyan, G. E., and M. A. Spall (2015), Wind-driven freshwater buildup and release in the Beaufort Gyre constrained by mesoscale eddies, *Geophys. Res. Lett.*, *42*, 273–282, doi:10.1002/2015GL065957.

McWilliams, J. (2008), The nature and consequences of oceanic eddies, in *Ocean Modeling in an Eddying Regime*, edited by M. W. Hecht, and H. Hasumi, pp. 5–15, AGU, Washington, D. C., doi:10.1029/177GM03.

Morison, J., R. Kwok, C. Peralta-Ferriz, M. Alkire, I. Rigor, R. Andersen, and M. Steele (2012), Changing Arctic Ocean freshwater pathways, *Nature*, *481*, 66–70, doi:10.1038/nature10705.

Nishino, S., M. Itoh, Y. Kawaguchi, T. Kikuchi, and M. Aoyama (2011), Impact of an unusually large warm-core eddy on distributions of nutrients and phytoplankton in the southwestern Canada Basin during late summer/early fall 2010, *Geophys. Res. Lett.*, *38*, L16602, doi:10.1029/2011GL047885.

Ou, H., and A. Gordon (1986), Spin-down of baroclinic eddies under sea ice, *J. Geophys. Res.*, *91*, 7623–7630, doi:10.1029/JC091iC06p07623.

Pickart, R., T. Weingartner, L. Pratt, S. Zimmermann, and D. Torres (2005), Flow of winter transformed Pacific water into the Western Arctic, *Deep Sea Res.*, *52*, 3175–3198, doi:10.1016/j.dsr2.2005.10.009.

Proshutinsky, A., and M. Johnson (1997), Two circulation regimes of the wind-driven Arctic Ocean, *J. Geophys. Res.*, *102*(C6), 12,493–12,514, doi:10.1029/97JC00738.

Proshutinsky, A., R. H. Bourke, and F. A. McLaughlin (2002), The role of the Beaufort Gyre in Arctic climate variability: Seasonal to decadal climate scales, *Geophys. Res. Lett.*, *29*(23), 2100, doi:10.1029/2002GL015847.

Proshutinsky, A., R. Krishfield, and D. Barber (2009a), Preface to special section on Beaufort Gyre Climate System Exploration Studies: Documenting key parameters to understand environmental variability, *J. Geophys. Res.*, *114*, C00A08, doi:10.1029/2008JC005162.

Proshutinsky, A., R. Krishfield, M.-L. Timmermans, J. Toole, E. Carmack, F. McLaughlin, W. Williams, S. Zimmerman, M. Itoh, and K. Shimada (2009b), Beaufort Gyre freshwater reservoir: State and variability from observations, *J. Geophys. Res.*, *114*, C00A10, doi:10.1029/2008JC005104.

Proshutinsky, A., D. Dukhovskoy, M.-L. Timmermans, R. Krishfield, and J. L. Bamber (2015), Arctic circulation regimes, *Philos. Trans. R. Soc.*, *373*(2052), 20140160, doi:10.1098/rsta.2014.0160.

Spall, M., R. Pickart, P. Fratantoni, and A. Plueddemann (2008), Western Arctic shelfbreak eddies: Formation and transport, *J. Phys. Oceanogr.*, *38*, 1644–1668.

Timmermans, M.-L., J. Toole, A. Proshutinsky, R. Krishfield, and A. Plueddemann (2008), Eddies in the Canada Basin, Arctic Ocean, observed from ice-tethered profilers, *J. Phys. Oceanogr.*, *38*(1), 133–145, doi:/10.1175/2007JPO3782.1.

Toole, J. M., R. A. Krishfield, M.-L. Timmermans, and A. Proshutinsky (2011), The ice-tethered profiler: Argo of the Arctic, *Oceanography*, *24*(3), 126–135, doi:10.5670/oceanog.2011.64.

Yang, J., A. Proshutinsky, and X. Lin (2016), Dynamics of an idealized Beaufort Gyre: 1. The effect of a small beta and lack of western boundaries, *J. Geophys. Res. Oceans*, *121*, 1249–1261, doi:10.1002/2015JC011296.

Zhao, M., and M.-L. Timmermans (2015), Vertical scales and dynamics of eddies in the Arctic Ocean's Canada Basin, *J. Geophys. Res. Oceans*, *120*, 8195–8209, doi:10.1002/2015JC011251.

Zhao, M., M.-L. Timmermans, S. Cole, R. Krishfield, A. Proshutinsky, and J. Toole (2014), Characterizing the eddy field in the Arctic Ocean halocline, *J. Geophys. Res. Oceans*, *119*, 8800–8817, doi:10.1002/2014JC010488.